# Correlation between Structure and Mass Distribution of the Nuclear Pore Complex and of Distinct Pore Complex Components

**R. Reichelt,* A. Holzenburg,* E. L. Buhle, Jr.,‡ M. Jarnik,* A. Engel,* and U. Aebi*§**

*M. E. Müller Institute for High Resolution Electron Microscopy at the Biocenter, University of Basel, CH-4056 Basel, Switzerland; ‡Department of Radiation Oncology, University of Pennsylvania School of Medicine, Philadelphia, Pennsylvania 19104; and §Department of Cell Biology and Anatomy, The Johns Hopkins University School of Medicine, Baltimore, Maryland 21205

***Abstract.*** Nuclear pore complexes (NPCs) prepared from *Xenopus laevis* oocyte nuclear envelopes were studied in "intact" form (i.e., unexposed to detergent) and after detergent treatment by a combination of conventional transmission electron microscopy (CTEM) and quantitative scanning transmission electron microscopy (STEM). In correlation-averaged CTEM pictures of negatively stained intact NPCs and of distinct NPC components (i.e., "rings," "spoke" complexes, and "plug-spoke" complexes), several fine structural features arranged with octagonal symmetry about a central axis could reproducibly be identified. STEM micrographs of unstained/freeze-dried intact NPCs as well as of their components yielded comparable but less distinct features. Mass determination by STEM revealed the following molecular masses: intact NPC with plug, 124 ± 11 MD; intact NPC without plug, 112 ± 11 MD; heavy ring, 32 ± 5 MD; light ring, 21 ± 4 MD; plug-spoke complex, 66 ± 8 MD; and spoke complex, 52 ± 3 MD. Based on these combined CTEM and STEM data, a three-dimensional model of the NPC exhibiting eightfold centrosymmetry about an axis perpendicular to the plane of the nuclear envelope but asymmetric along this axis is proposed. This structural polarity of the NPC across the nuclear envelope is in accord with its well-documented functional polarity facilitating mediated nucleocytoplasmic exchange of molecules and particles.



THE nuclear pore complex (NPC)[1] is an elaborate membrane-bound organelle integrated in the nuclear envelope of all eukaryotic cells, where it is interposed between the inner and outer nuclear membrane (for recent reviews see Newport and Forbes, 1987; Gerace and Burke, 1988). The density of NPCs within the nuclear envelope of *Xenopus laevis* oocytes, for example, is ~60 pores/$\mu m^2$ (Kartenbeck et al., 1971; Maul, 1977). In negative stain, the apparent diameter of the NPC is typically 120 nm (Franke, 1974; Unwin and Milligan, 1982; Milligan, 1986). NPCs are widely believed to represent the sites of nucleocytoplasmic exchange of molecules and particles (see Dingwall and Laskey, 1986; Newport and Forbes, 1987; Gerace and Burke, 1988; Feldherr and Dworetzky, 1988; Zimmer et al., 1988). Passive diffusion of small molecules or particles of known diameter evaluated by cytoplasmic microinjection of dextrans, polyvinylpyrrolidone-coated colloidal gold, and soluble proteins suggests the presence of a channel with a physical opening of ~9 nm in diameter acting as a molecular sieve (Bonner, 1975*a*; Paine et al., 1975; Feldherr and Dworetzky, 1988). Translocation of metabolically labeled polypeptides (Bonner, 1975*b*; Feldherr, 1975; DeRobertis et al., 1978), nuclear proteins such as nucleoplasmin (Dingwall et al., 1982), and nucleoplasmin- and RNA-coated gold particles of various sizes (Feldherr et al., 1984; Dworetzky and Feldherr, 1988) through the nuclear pores of amphibian oocytes has established a NPC channel with a functional diameter of 23–26 nm facilitating mediated transport.

Since early structural studies of the NPC (Gall, 1967; Franke and Scheer, 1970) it has widely been agreed that it consists of eight structural units arranged with pronounced octagonal symmetry about an axis perpendicular to the nuclear membrane plane. However, the consistently poor state of preservation of NPC preparations has resulted in a wide range of structural models describing the fine structure of the NPC (see Abelson and Smith, 1970; Wunderlick and Speth, 1972; Franke, 1974; Hoeijmakers et al., 1974; Harris, 1974, 1978). Ultimately, a more generally accepted working model of the NPC has been proposed by Unwin and Milligan (1982) based on a three-dimensional (3D) reconstruction to ~9 nm resolution computed from "intact" NPCs (i.e., without detergent treatment) together with interpretation of edge-on views of NPCs after detergent treatment. This model reveals several reproducible NPC components, all arranged

1. *Abbreviations used in this paper*: CTEM, conventional transmission electron microscopy; LSB, low-salt buffer; NPC, nuclear pore complex; RMP, radial mass profile; STEM, scanning transmission electron microscopy.

with octagonal symmetry about a central axis perpendicular to the nuclear envelope. Starting from the center of the NPC, the distinct components have been referred to as "plug," eight radially protruding "spokes," and two equal "rings" facing the cytoplasm and the nucleoplasm, respectively. Whereas the 3D reconstruction suggests that the basic framework of the intact NPC consists of two equal but oppositely facing halves, the overall mass density yields a pronounced asymmetry towards the cytoplasmic face of the NPC, which Unwin and Milligan attribute to the specific "decoration" of the cytoplasmic ring with eight "22-nm particles," possibly representing ribosomes.

Stewart and Whytock (1988) have examined the structure of the nuclear envelope of *Xenopus laevis* oocytes before and after detergent extraction by EM of metal-shadowed specimens both after freeze drying and air drying. Accordingly, the cytoplasmic face of the nuclear envelope contains roughly cylindrical NPCs that are decorated with distinct granules on their uppermost face and are often linked by pore-connecting fibrils. The nucleoplasmic face of the same preparations reveals a fibrous lamina (i.e., the nuclear lamina; see Gerace, 1986; Aebi et al., 1986; Gerace and Burke, 1988) appearing as a canopy supported by the NPCs. In addition, disruption of NPCs after detergent treatment of nuclear envelopes yields rings which, sometimes, further dissociate into linear arrays of subunits like beads on a string.

Recently, cryoelectron microscopy of frozen-hydrated NPCs has yielded a refined model describing the modular architecture of the NPC at 6 nm resolution (Akey, 1989; Akey and Goldfarb, 1989). Features worth mentioning in this model are the radial arms projecting out past the membrane border, possibly representing membrane-anchoring sites, thus giving the NPC an effective diameter of ~145 nm. Akey's NPC model, although based on projection data only, assumes a symmetric overall mass distribution relative to the nuclear envelope. Most interesting are the results about the central plug, which can assume distinct transport-related structural states, i.e., an "open" and a "closed" state. Hence the central plug is implicated to represent the actual "transporter" for nucleocytoplasmic exchange of molecules and particles (Akey and Goldfarb, 1989).

In contrast to the wealth of experimental data about the structure of the NPC, comparably little and rather diverse data, sometimes highly speculative, have been published concerning its mass. The NPC is believed to be mostly composed of protein, and from its overall size may contain 100–200 polypeptides with average molecular masses of ~50 kD. Thus its total protein mass may be on the order of 10 MD (Franke, 1974; Fry, 1976; Maul, 1977). Although Blobel (1985) estimated its mass to be on the order of 100 MD based on the dimensions measured by Unwin and Milligan (1982), Gerace and Burke (1988) speculated that the total molecular mass of the NPC be in the range of 25 to 100 MD. Krohne et al. (1978) tried to actually measure NPC masses. The averages for different preparations ranged from $1.76 \cdot 10^{-16}$ to $2.45 \cdot 10^{-16}$ (i.e., 110–148 MD) for unfixed NPCs and to $2.59 \cdot 10^{-16}$ (i.e., 160 MD) for glutaraldehyde-fixed NPCs.

Here we present results obtained by combining structural data yielded from conventional transmission EM (CTEM) with mass maps revealed by scanning transmission EM (STEM; Engel, 1978; Engel et al., 1982) in a way that allows their direct comparison, thus providing further insight into the supramolecular architecture of this complex organelle and its components and both complementing and extending our understanding of the recently proposed models (i.e., Unwin and Milligan, 1982; Milligan, 1986; Akey, 1989; Akey and Goldfarb, 1989). Finally, we present experimental mass values of several distinct NPC components together with their respective radial mass profiles.

## Materials and Methods

### Isolation of Nuclear Envelopes and Preparation of Intact NPCs

Mature oocytes were isolated from *Xenopus laevis* and stored in modified Barth's saline at 4°C for ≤2 wk. Modified Barth's saline contained 88 mM NaCl, 1 mM KCl, 0.82 mM $MgSO_4$, 0.33 mM $Ca(NO_3)_2$, 0.41 mM $CaCl_2$, 10 mM Hepes, pH 7.5, and 100 U/ml of penicillin-streptomycin (Gibco Laboratories, Grand Island, NY). Before use, individual oocytes were equilibrated at room temperature and washed three times in a low-salt buffer (LSB) containing 0.5 mM $MgCl_2$, 1 mM KCl, and 10 mM Hepes, pH 7.5, as well as traces of PMSF. After the oocytes were placed in a small petri dish filled with LSB, the nuclei were manually isolated under an obliquely lighted dissecting microscope using forceps and an adjustable (2.5–5 μl) pipette. The forceps were used to gently break open the oocytes along a line between the vegetal and animal pole or, alternatively, to puncture a hole in the oocyte at its animal pole. Pipette suction was used to both manipulate and clean the nuclei of contaminating yolk particles and other debris. Next, the intact nucleus was taken up in the pipette tip and injected into a 5–10-μl droplet of LSB placed on a carbon-coated collodion film deposited on a 400-mesh copper grid with the carbon film pointing towards the nucleus. After allowing the nucleus to settle by gravity onto the support film, it was ruptured and gently spread across the grid using fine glass needles that had been drawn from micropipettes on a microelectrode puller. The thus spread nuclear envelope, with its cytoplasmic side facing the carbon support film, was either washed with double-distilled water (3 × 2.5 μl) for 10 s, with LSB (3 × 2.5 μl) for 30 s, or with two droplets of LSB for 10 min. After each washing step, excessive liquid was drained off towards the edge of the grid. The last washing step was immediately followed by a fixation step (see Preparation of Specimens for EM).

### Preparation of Detergent-treated NPCs

To obtain detergent-treated NPCs, spread envelopes (see previous paragraph) were subjected to detergent extraction: four 2.5-μl droplets of LSB containing 0.1% Triton X-100 were applied for 15–60 s each, followed by four 5–10-s washes with 2.5-μl droplets each of LSB containing 0.1% ethanol. After each application of either detergent or wash solution, excessive liquid was drained off. All extractions were performed at pH 7.4 and at 25°C.

### Preparation of Specimens for EM

For CTEM, specimens were chemically fixed and negatively stained as follows: a 2.5-μl droplet of fixing solution was applied to the grid. After two renewals and a total fixation time of 10 min at 25°C, the specimens were negatively stained (omitting the last washing step in LSB) with 0.75% uranyl formate, pH 4.25 (Buhle et al., 1983). The fixing solution consisted of LSB containing 0.8% glutaraldehyde and 2% paraformaldehyde, or just 4% glutaraldehyde. All fixing solutions were freshly prepared immediately before use.

For STEM, specimens were prepared as detailed above, but on a 4-nm carbon film supported by a fenestrated thick carbon layer deposited on a 400-mesh copper grid (Engel and Meyer, 1980). After mounting, tobacco mosaic virus, serving as an internal mass standard (Wall, 1979), was adsorbed for 30 s from a 2.5-μl droplet, before excess liquid was removed, and the grid was thoroughly washed on three droplets of quartz-distilled water with a blotting step between each wash. Immediately following, the sample was frozen in liquid $N_2$, transferred to a freeze-drying chamber directly attached to the STEM, and freeze-dried overnight at −90°C.

## EM

Negatively stained samples were examined in a transmission electron microscope (model H-7000; Hitachi Ltd., Tokyo, Japan) operated at 100 kV, equipped with a liquid-nitrogen cooled anticontamination device and a low-dose kit. Micrographs were recorded on electron image sheet film (SO-163; Eastman Kodak Co., Rochester, NY) at a nominal magnification of 20,000× and developed for 6 min in threefold diluted D-19 (Eastman Kodak Co.). Magnification was calibrated according to the method of Wrigley (1968) using negatively stained catalase crystals.

Elastic annular dark-field (DF) images containing 512 × 512 pixels were acquired in digital form using a (Model HB-5; Vacuum Generators Microscopes Ltd., East Grinstead, UK) STEM operated at 80 kV at either 50,000× (pixel size 3.68 nm) or 100,000× (pixel size 1.84 nm) nominal magnification and at doses between 50 and 300 $e^-/nm^2$ (Engel, 1978).

## Digital Image Processing

Images of negatively stained NPCs recorded at 20,000× nominal magnification were digitized using an imaging camera (850 CCD; Eikonix Corp., Bedford, MA). The scanner signal was averaged over 2 × 2 pixels to yield a final sampling raster of 22.6 × 22.6 μm on the micrograph, corresponding to a pixel size of 1.13 × 1.13 nm at the specimen level. For the extraction of single NPCs, a standard box of 128 × 128 pixels was centered around each NPC, and the pixel values contained within this box were saved on disk. This interactive method permitted rapid scanning of large micrograph areas and selection of individual NPCs based on their overall appearance. The criteria for selection were (*a*) even negative staining and (*b*) minimal deviation from octagonal symmetry. Subfiles were processed using iterative angular and translational alignment routines provided by the SEMPER VI software package (Saxton et al., 1979) run under VMS on a DEC VAX 8200 computer (Digital Equipment Co., Marlboro, MA). Processing of digital STEM data for mass determination was carried out as described (Engel, 1978; Engel and Reichelt, 1988). To establish mass maps of the intact NPC and of several of its distinct components, digital images of individual particles were selected by eye for correlation averaging. Particles exhibiting octagonal symmetry were aligned and processed according to the procedures mentioned above.

## Evaluation of the Background: the Contribution of the Nuclear Envelope

To determine the mass of the intact NPCs that were embedded in the nuclear envelope, the mass contributed by the nuclear envelope had to be subtracted from the NPC mass measured by integration over a circular area with a diameter of 120 nm (Table I). To this end, the nuclear membrane was assumed to wrap around the NPC to maintain continuity between the outer and inner nuclear membrane in a circularly curved fashion (Fig. 8) with a mean radius of 30 nm, based on a mean nuclear envelope thickness of 65 nm (Franke, 1974; our own measurements) and a mean nuclear membrane thickness of 6 nm (Franke, 1974), thus forming a hole within the nuclear envelope with a diameter of ~90 nm (see Unwin and Milligan, 1982; Newport and Forbes, 1987; Akey, 1989). With this geometry, the nuclear membrane piece embracing the NPC is a circular torus segment that has a surface area of ~22,000 $nm^2$. By coincidence, this is close to the nuclear envelope double membrane occupied by a 120-nm-diam NPC. The mass/area of the nuclear envelope was evaluated for a number of intact nuclear envelope patches (~2 $\mu m^2$ each) by punching out the circular 120-nm diameter areas occupied by the NPCs and simply integrating the mass values over the punctate envelope and dividing this sum by the corresponding nuclear envelope area.

# Results

## Preparation and Structural Analysis of Intact and Detergent-treated NPCs

To avoid the uncontrolled contribution of heavy metal in the STEM mass analysis of intact and detergent-treated NPCs, we had to omit the $OsO_4$ fixation step used by Unwin and Milligan (1982) aimed at optimally preserving NPCs for structural analysis. This, in turn, meant that we also had to analyze the negatively stained material in the CTEM without

*Table I. Data of Unfixed Intact NPC and of Distinct NPC Components after Detergent Treatment Prepared from Xenopus laevis Oocyte Nuclear Envelopes*

| Complex | Mass | Diameter (STEM)* (unfixed) | Diameter (CTEM)* (chemically fixed) |
|---|---|---|---|
| | *MD* | *nm* | *nm* |
| NPC with plug (membrane-detached) | 125.0 ± 12.0 (210) | $D_o$ = 122.2 ± 5.7 | |
| NPC with plug (membrane-bound) | 124.0 ± 11.0 (207) | $D_o$ = 121.0 ± 4.5‡ | $D_o$ = 116.3 ± 8.1‡ |
| NPC without plug (membrane-bound) | 112.0 ± 11.0 (201) | | |
| Plug ([NPC + P] − [NPC − P]) | 12.0 ± 1.1§ | $D_o$ = 44.0 ± 4.0 | $D_o$ = 30.6 ± 5.0 |
| Plug-spoke | 65.7 ± 8.3 (48) | $D_o$ = 120.5 ± 4.3‡ | $D_o$ = 115.8 ± 6.5‡ |
| Spoke | 51.7 ± 5.3 (45) | | |
| Plug [PS − P] | 14.0 ± 1.4§ | $D_o$ = 41.0 ± 4.0 | $D_o$ = 30.6 ± 5.0 |
| "Heavy" ring (cytoplasmic) | 32.0 ± 5.5 (224) | $D_o$ = 122.0 ± 4.1‡ | $D_o$ = 118.9 ± 8.5‡ |
| "Light" ring (nucleoplasmic) | 21.1 ± 3.7 (81) | $D_o$ = 59.5 ± 3.0‡ | $D_o$ = 76.7 ± 4.3‡ |
| "Light" particle | 6.0 ± 2.8 (200) | $D_o$ = 23.0 ± 2.3 | $D_o$ = 27.3 ± 3.6 |
| "Heavy" particle | 12.6 ± 2.8 (198) | $D_o$ = 32.4 ± 2.4 | $D_o$ = 27.3 ± 3.6 |

The SDs (± values) are given for directly measured data; numbers of particles included for mass determination are given in brackets. The mass of the plug was calculated as the difference of (*a*) intact NPC with plug minus intact NPC without plug, and (*b*) plug-spoke minus spoke. Abbreviations used: $D_o$, outer diameter; $D_i$, inner diameter; *P*, plug; *PS*, plug-spoke.

* In each case, mean values were calculated from ~40 particles.

‡ Diameters of both types of particles were statistically indistinguishable.

§ Uncertainties were evaluated according to the Gaussian law of error propagation.

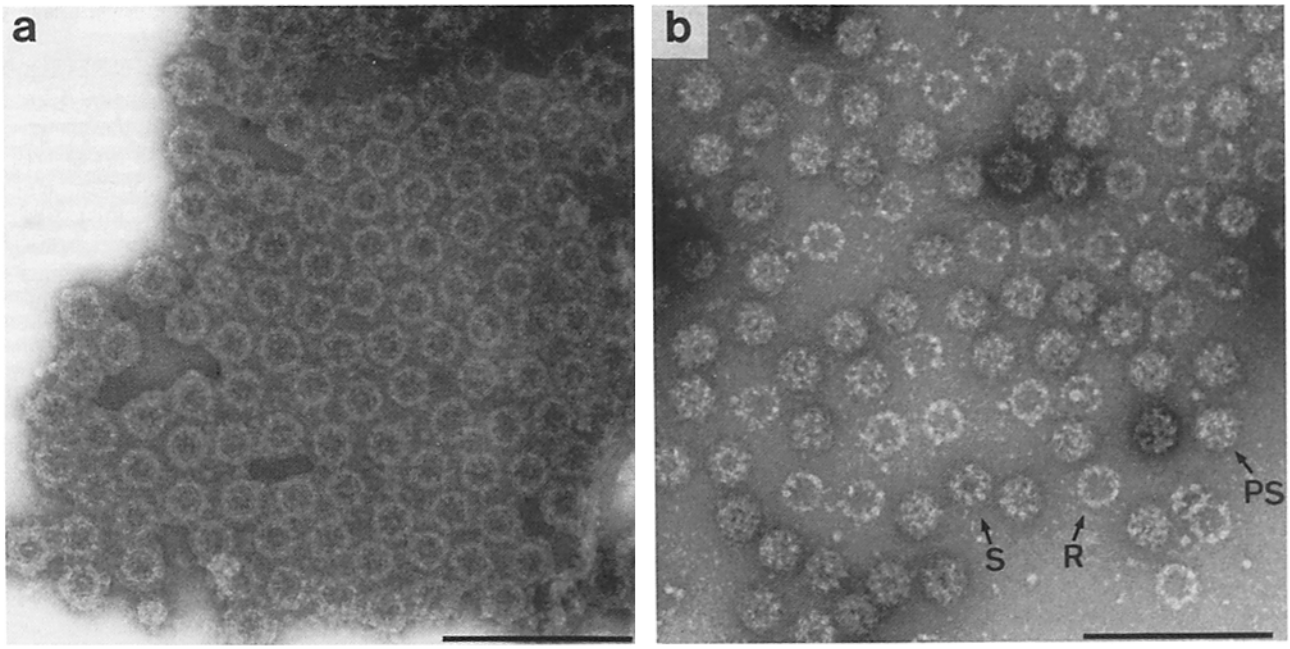


*Figure 1.* CTEM images of negatively stained intact (*a*) and detergent-treated (*b*) NPCs prepared from spread nuclear envelopes manually isolated from *Xenopus laevis* oocytes. Whereas the intact NPCs in *a* are embedded in the nuclear envelope, the detergent-treated NPCs in *b* have detached from the nuclear envelope and are directly adsorbed to the support film. As illustrated in *b*, detergent treatment leads to disintegration of the intact NPCs into three distinct NPC components, i.e., plug–spoke complexes (*PS*), spoke complexes (*S*), and rings (*R*). Both preparations (*a* and *b*) were processed without $OsO_4$ fixation and negatively stained with 0.75% uranyl formate, pH 4.25. To minimize beam-induced radiation damage, all micrographs were recorded under low-dose conditions (≤2,000 $e^-/nm^2$). Bars, 500 nm (*a* and *b*).

$OsO_4$ fixation to allow for comparison of the CTEM with the STEM data.

Fig. 1 displays representative areas of intact (Fig. 1 *a*; i.e., without exposure to detergent) and detergent-treated (Fig. 1 *b*) NPCs, which have been prepared from *Xenopus laevis* oocyte nuclear envelopes directly spread onto EM grids by a procedure similar to that described by Unwin and Milligan (1982), however omitting the $OsO_4$ fixation step, and negatively stained with 0.75% uranyl formate instead of 1% uranyl acetate or 2% gold thioglucose (see Materials and Methods). As documented with Fig. 1 *a*, intact NPCs prepared in this manner are primarily found in nuclear envelope membrane patches where they are relatively densely but usually irregularly packed, with their cytoplasmic side facing the support film. While absent in the example shown, a quasi-tetragonal nuclear lamina meshwork, lining the inner nuclear membrane in situ, sometimes appears superimposed onto the NPC-containing membrane patches (see Aebi et al., 1986; Stewart and Whytock, 1988). The appearance of thus prepared NPCs is dominated by a ~120-nm outer diameter "annulus" exhibiting pronounced octagonal symmetry about a central axis.

When nuclear envelopes spread on an EM grid were extracted for one to several minutes with LSB buffer containing 0.1% Triton X-100 before washing and negatively staining them (see Materials and Methods), sample areas such as presented in Fig. 1 *b* were commonly observed. Such detergent treatment apparently led to disintegration of the intact NPCs into three distinct NPC components, all exhibiting pronounced octagonal symmetry about a central axis: "plug–spoke" (PS) complexes, "spoke" (S) complexes, and "rings" (R). Unlike intact NPCs (see Fig. 1 *a*), these NPC components were no longer embedded in the nuclear envelope but were directly stuck to the EM support film. Sometimes they did occur, however, next to still more or less intact nuclear envelope fragments (not shown), suggesting that they might have been "released" from the nuclear envelope upon detergent treatment (see also Fig. 3 from Unwin and Milligan, 1982). As documented in Fig. 2, from the stain penetration patterns depicted in 45° and 60° tilted views, it becomes obvious that the plug–spoke and spoke complexes yielded after detergent treatment are no longer framed between rings but are free-standing entities exhibiting a fair degree of vorticity, a finding in contrast with earlier interpretations of these complexes when viewed edge-on (Unwin and Milligan, 1982; Akey, 1989).

To determine the common and reproducible structural features (i.e., those not subject to modulation by specimen preparation) of intact and detergent-treated NPCs, we computed correlation-averaged images (see Materials and Methods) of intact NPCs, plug–spoke complexes, spoke complexes, and rings. Due to the strong eightfold angular harmonics in the power spectra of these averages, their eightfold symmetrization about a central axis appeared justified. The resulting images are displayed in Fig. 3. Examination of correlation-averaged negatively stained intact NPCs (Fig. 3 *a*) reveals several prominent features including a strong "outer annulus" with a mean outside diameter of ~116 nm (Table I), and eight wedge-shaped "spokes' projecting inwards from the outer annulus towards a faint narrow "inner annulus" with

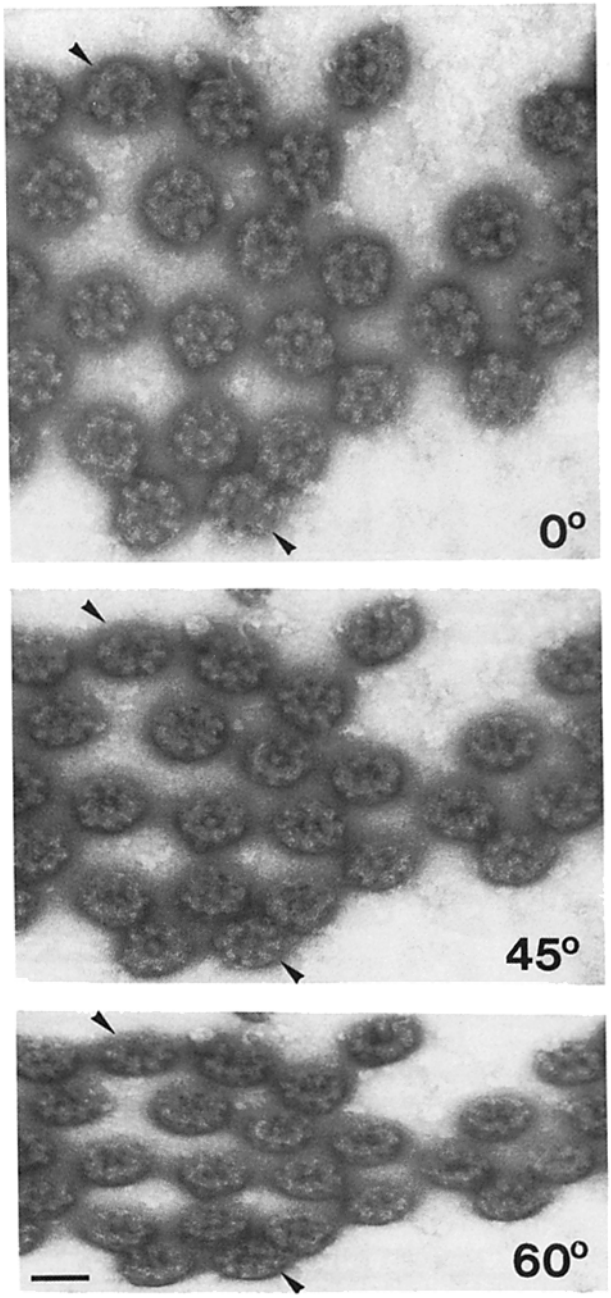


*Figure 2.* CTEM 0°/45°/60° tilt series of negatively stained detergent-treated NPCs prepared and processed as described in Fig. 1. Two representative particles have been identified with arrowheads throughout the tilt series. From the tilted views it becomes obvious that the detergent-treated NPCs are devoid of rings. As in Fig. 1, each micrograph within the tilt series was recorded under low-dose conditions (≤2,000 $e^-/nm^2$). Bar, 100 nm.

a mean diameter of ~60 nm, probably corresponding to the "inner spoke ring" depicted by Akey (1989) in frozen-hydrated NPCs. A significant fraction of the intact NPCs exhibit indications of a stain excluding "central plug" (Fig. 1 *a*), which in correlation-averaged images (Fig. 3 *a*) yields a mean diameter of ~31 nm (Table I). Frequently, arm-like structures can be discerned that appear to emanate from the outer annulus (Fig. 1 *a*); however, they were not sufficiently ordered and reproduced from NPC to NPC to make a significant contribution to the correlation-averaged NPC image (Fig. 3 *a*).

Comparison of the correlation-averaged intact NPC (Fig. 3 *a*) with detergent-treated NPCs (Fig. 3, *b–d*) yields some striking changes. In contrast to the intact NPC, the prominent spokes seen in both the plug-spoke (Fig. 3 *b*) as well as the spoke (Fig. 3 *c*) complex appear to extend further radially inward hence forming a distinct "plug-surrounding ring" having a mean diameter of ~56 nm. It is conceivable that this plug-surrounding ring corresponds to the inner annulus faintly visible in intact NPCs (see above, and Fig. 3 *a*). Detergent treatment not only disassembles the NPC into distinct components, but it also increases its accessibility to the negative stain. Thus, in detergent-treated NPCs the central plug and the plug-surrounding ring become more clearly visible than in intact NPCs and, in addition, some fine structure of the spoke is unveiled that is virtually the same for the plug–spoke (Fig. 3 *b*) and the spoke (Fig. 3 *c*) complex. Accordingly, each spoke is subdivided into three morphological domains, with the innermost domains of adjacent spokes joining each other to form the plug-surrounding ring (see above). Both types of complexes yield an average outermost diameter of 116 nm (Table I), and they both exhibit a significant vorticity (Fig. 3, *b* and *c*) indicating a difference between their cytoplasmic and nucleoplasmic halves (see Discussion and Fig. 8). Correlation-averaged and eightfold rotationally symmetrized images of negatively stained rings (Fig. 3 *d*) yield an apparent outer diameter of ~119 nm and an apparent inner diameter of ~77 nm (Table I). In fact, the overall size and shape of the rings appear quite similar to the outer annulus dominating the intact NPC images (see above, and Fig. 3 *a*).

### *STEM Analysis of Intact and Detergent-treated NPCs*

To determine the respective masses of the intact NPC and of its distinct components, we used quantitative STEM on freeze-dried, unfixed, and unstained preparations of intact (Fig. 4 *a*) and detergent-treated (Fig. 4, *b* and *c*) NPCs. As expected for unstained samples recorded at doses between 50 and 300 $e^-/nm^2$, the unprocessed images in Fig. 4 reveal much less structural detail than those of the corresponding negatively stained samples (compare with Figs. 1 and 2). Nevertheless, the same types of structures could be recognized, i.e., intact NPCs with or without a central plug (Fig. 4, *a*, *d*, and *e*), rings (Fig. 4, *b*, *c*, and *g*), plug–spoke (Fig. 4 *c*) and spoke (Fig. 4, *c* and *f*) complexes. It appears that in the case of unstained intact NPC preparations (Fig. 4 *a*) the difference between NPCs with (Fig. 4 *d*) and without (Fig. 4 *e*) a central plug is more pronounced than in negatively stained intact NPC preparations (Fig. 1 *a*). This may be a consequence of the relative surface topographies of the central versus annular parts of this organelle, thus causing preferential stain accumulation in the center and hence "burying" the plug under the stain. Sometimes, images of unprocessed intact NPCs (Fig. 4, *a*, *d*, and *e*) or rings (Fig. 4, *b*, *c*, and *g*) exhibit a hint of octagonal symmetry about a central axis that is manifested as distinct eightfold angular harmonics in corresponding power spectra. As marked in Fig. 4 *b*, two types of rings can be distinguished in detergent-treated samples, i.e., "heavy" rings ($R_h$, i.e., appearing bright) and "light" rings ($R_l$, i.e., appearing dimmer). The heavy rings are found significantly more frequently than the light rings,

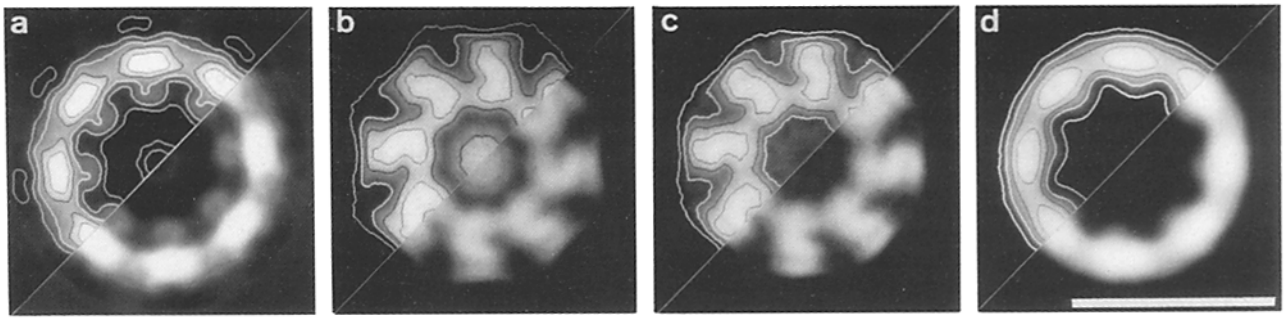


*Figure 3.* Correlation-averaged and eightfold rotationally symmetrized CTEM images of negatively stained intact (*a*) and detergent-treated (*b–d*) NPCs prepared and recorded as described in Fig. 1. (*a*) Intact NPC ($n$ = 18), (*b*) plug–spoke complex ($n$ = 33), (*c*) spoke complex ($n$ = 39), and (*d*) ring ($n$ = 46). To emphasize some of the fine structural details, contours have been superimposed onto one-half of each averaged particle image. $n$ denotes the number of particles included in each average. Bright areas represent stain exclusion (i.e., protein); dark areas represent negative stain. Bar, 100 nm (*a–d*).

typically 80 versus 20% (see Discussion). Fig. 4, *d–g* display unprocessed single particle images of an intact NPC with plug (*d*), an intact NPC without plug (*e*), a spoke complex (*f*), and a heavy ring (*g*). As can be seen in Fig. 4 *c*, particle "pairs" consisting of a ring and a plug–spoke or a spoke complex often come to lie next to each other indicating that they may have originated from one and the same intact NPC after disintegration. Moreover, "bright granules" with diameters ranging from 20 to 35 nm (Fig. 4, *b* and *c*) are often lying next to such disintegrated NPCs, but occur much less frequently further away, and hence may represent NPC-related particles.

The respective masses of the different NPC structures defined above have all been evaluated by quantitative STEM as described in Materials and Methods. To document the quality of these mass measurements, two representative mass histograms, i.e., those for intact membrane-detached NPCs (Fig. 5 *a*) and heavy rings (Fig. 5 *b*), are shown. The average mass values together with their SDs computed from such histograms are listed in Table I. Accordingly, the total mass of the intact NPC with central plug (e.g., Fig. 4 *d*) amounts to 124 MD and that without plug (e.g., Fig. 4 *e*) to 112 MD, thus yielding a mass of 12 MD for the central plug, i.e., when assuming it to be represented by the difference of the two distinct NPC moieties. Similarly, the total mass of the plug–spoke complex is 66 MD and that of the spoke complex (e.g., Fig. 4 *f*) 52 MD, thus yielding a mass of 14 MD for the central plug. The heavy ring (e.g., Fig. 4 *g*) has a total mass of 32 MD, whereas the light ring measures 21 MD. Based on their masses and diameters, two types of NPC-related particles could be distinguished, i.e., "light" particles with an average mass of 6 MD and an average outer diameter of 23 nm, and "heavy" particles with an average mass of 13 MD and an average outer diameter of 32 nm (see Table I). As can be depicted in Fig. 4 *c*, the heavy rings appeared to frequently be decorated with one to several particles. The average mass of 32 MD only included heavy rings with no indication of particles decorating them. We did, however, determine the mass of heavy rings containing one or two particles and from those calculated the average particle mass to be 6.7 MD, i.e., by subtracting the average mass of the undecorated rings, a value close to that of the "light" particles (see above and Table I).

In Fig. 6, correlation-averaged STEM images of unstained/freeze-dried intact and detergent-treated NPCs are displayed. Comparison of these "mass maps" with the corresponding averages of CTEM images of negatively stained NPC structures (Fig. 3) yields good agreement in terms of overall dimensions (Table I) and low-resolution structural features. Due to the clear distinction between images of intact NPCs with (Fig. 4 *d*) and without (Fig. 4 *e*) central plug, two separate averages were computed (Fig. 6, *a* and *b*). Accordingly, the diameter of the central plug, i.e., that enclosing a mass of 12 MD, is 44 nm (Table I). The NPC components exhibiting the best preserved octagonal symmetry are the rings (Fig. 6, *c* and *d*). The smoother appearance of the heavy-ring average (Fig. 6 *c*) compared with that of the light ring average (Fig. 6 *d*) is primarily due to the approximately four times larger number of heavy rings included in the average. In the case of the plug–spoke and spoke complexes the preservation of eightfold rotational symmetry was too poor to be enforced, and therefore the corresponding mass maps have not been displayed.

To obtain a more quantitative view of the radial distribution of mass projected perpendicular to the nuclear envelope plane of the different intact and detergent-treated NPC structures, radial mass profiles (RMPs), corrected for signal nonlinearities due to plural scattering (Reichelt and Engel, 1984), were computed from the corresponding mass maps and are presented in Fig. 7. Accordingly, the RMPs of intact NPCs with (Fig. 7 *a*) and without (Fig. 7 *b*) central plug are almost identical for radii >20 nm, documenting that the major difference between the two forms is indeed the presence or absence of a central plug that, in turn, is confined to radii ≤20 nm. Similarly, the RMPs of the plug–spoke (Fig. 7 *c*) and spoke (Fig. 7 *d*) complexes differ from each other in the same way. The radial position of the major shoulder in the different RMPs is ~35 nm for Fig. 7, *a* and *b*, ~22 nm for Fig. 7 *d*, and ~44 nm for Figs. 7, *e* and *f*. Adding the heavy- (Fig. 7 *e*) and light- (Fig. 7 *f*) ring RMPs to that of the plug–spoke complex (Fig. 7 *c*) yields to a good approximation the RMP of the intact NPC with central plug (Fig. 7 *g*), and similarly, adding the two-ring RMPs to that of the spoke complex (Fig. 7 *d*) roughly yields the RMP of the intact NPC without central plug (Fig. 7 *h*). Finally, by assuming a mean protein density of 813 D/nm$^3$, the major shoulders of the

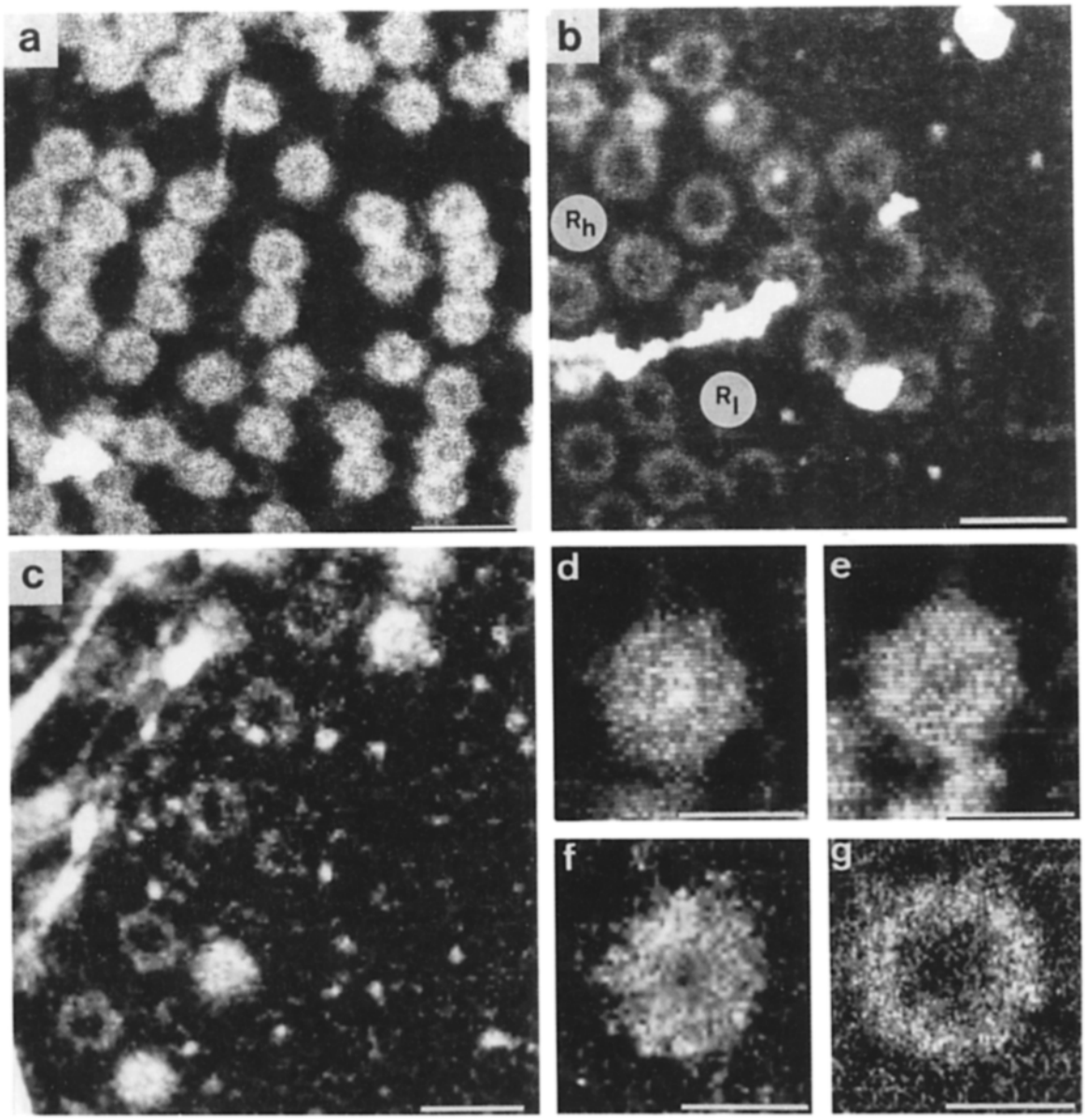


*Figure 4.* Elastic annular dark-field STEM images of freeze-dried, unstained, and completely unfixed intact (*a*, *d*, and *e*) and detergent-treated (*b*, *c*, *f*, and *g*) NPCs digitally recorded at low doses (50 to 300 $e^-/nm^2$). (*a*) Nuclear envelope with embedded intact NPCs spanning a fissure in the carbon support film. Such "unsupported" areas were used for mass determination. (*b*) Distinct NPC components revealed after detergent treatment of the material shown in (*a*) directly adsorbed to a 4-nm-thick carbon support film. The following structures can be distinguished: "heavy" rings ($R_h$; bright rings), "light" rings ($R_l$; dimmer rings), and "particles" (bright spherical dots, diameter ~20–35 nm). (*c*) Same preparation as in *b* depicting "complementary" NPC components consisting of a heavy ring and a plug-spoke or spoke complex. (*d–g*) Higher magnification en face views of an intact NPC with plug (*d*), an intact NPC without plug (*e*), a spoke complex (*f*), and a heavy ring (*g*). Bars, 200 nm (*a–c*), and 100 nm (*d–g*).

RMPs of intact NPCs (i.e., Fig. 7, *a* and *b*) correspond to a mass thickness of ~50 nm, those of the RMP of the spoke complex (i.e., Fig. 7 *d*) to ~43 nm, and the central peak of the RMP of the intact NPC with spoke (i.e., Fig. 7 *a*) to ~56 nm. Note, however, that these mass thicknesses represent minimal dimensions of the corresponding NPC structural features perpendicular to the nuclear envelope plane, as they are based on a compact mass distribution in this direction without assuming voids or cavities.

## Discussion

Combination of CTEM data obtained from negatively stained intact and detergent-treated NPCs prepared from *Xenopus laevis* oocyte nuclear envelopes with quantitative STEM data of the corresponding unstained/freeze-dried structures has yielded a refined view of the complex NPC architecture together with its biophysical characterization in terms of total mass, mass maps, and radial mass profiles.

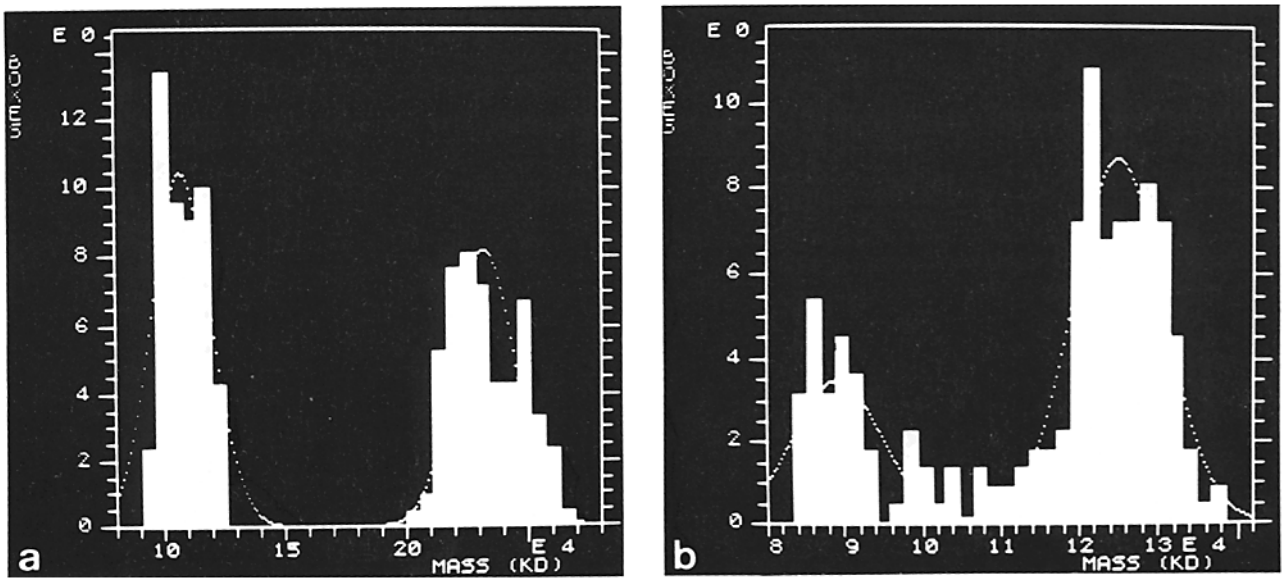


*Figure 5.* STEM mass histograms of membrane-detached intact NPCs (*a*) and heavy rings (*b*). In both histograms the left peak represents the mass distribution of empty carbon support film, while the right peak represents the mass distribution of particles plus carbon support film. Gaussian profiles were fitted to the experimental mass distributions using a Marquardt fitting algorithm (Bevington, 1969) yielding peak positions as well as standard deviations. The average masses of the intact NPC and the heavy ring are given by the difference of the two peak positions in each histogram.

To avoid uncontrolled mass contributions by heavy metal, all NPC preparation steps were performed in the absence of $OsO_4$. The characteristic dimensions of the intact NPC and its distinct components after detergent treatment (i.e., plug–spoke and spoke complexes, rings, and plugs) evaluated by this study (see Table I) agree within ⩽5% with those of corresponding $OsO_4$-treated NPCs (Unwin and Milligan, 1982; Buhle et al., 1985). For example, the outer diameter of intact NPCs is 116 nm (Table I), versus a published value of 120 nm. Similarly, the outer diameter of the rings is 119 (Table I) vs. 120 nm as published. In addition, a study using different negative stains (Jarnik, M., E. L. Buhle, R. Reichelt, A. Holzenburg, A. Engel, and U. Aebi, manuscript in preparation) has yielded plug–spoke and spoke complexes with an average outer diameter of 116 nm, irrespective of whether $OsO_4$ was used (data not shown) or not (Fig. 3, *b* and *c*; Table I). Even such fine structural details as the partitioning of the spokes into three domains (Fig. 3, *b* and *c*) closely matches previously published data by Unwin and Milligan (1982) and by Akey (1989). Accordingly, the inner domain is placed at 20–38 vs. 22–40 nm, the middle domain at ~42 vs. 45 nm, and the outer domain at ~51 vs. 55 nm. In conclusion, the absence of $OsO_4$ does not seem to seriously handicap structural investigations of the NPC at a resolution of 5–10 nm.

One significant difference from previously published NPC data is our interpretation of NPCs after detergent treatment. Whereas Unwin and Milligan (1982) as well as Akey (1989), mainly based on edge-on views occasionally found in such preparations, concluded that detergent-treated NPCs still

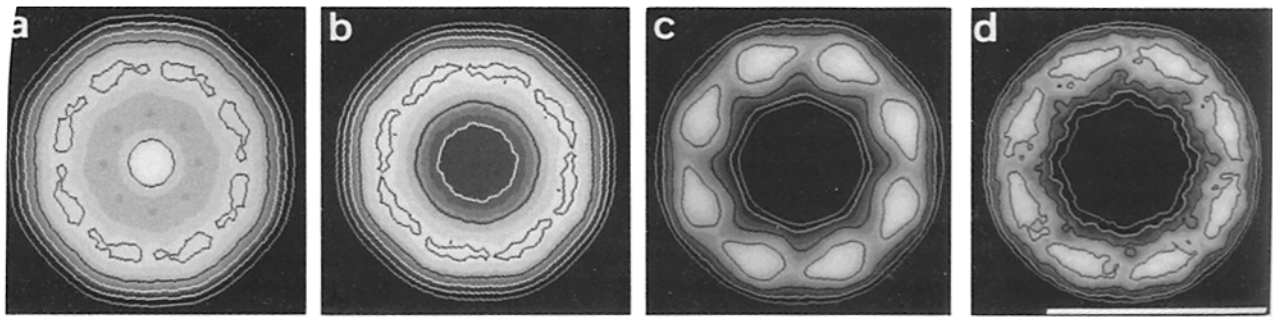


*Figure 6.* Correlation-averaged and eightfold rotationally symmetrized elastic annular dark-field STEM images (i.e., mass maps) of freeze-dried, unstained, and completely unfixed intact (*a* and *b*) and detergent-treated (*c* and *d*) NPCs prepared and digitally recorded as described in Fig. 4. (*a*) Intact NPC with plug ($n$ = 49), (*b*) intact NPC without plug ($n$ = 46), (*c*) heavy ring ($n$ = 51), and (*d*) light ring ($n$ = 16). The average contributions of the nuclear envelope (*a* and *b*) and the carbon support film (*c* and *d*), respectively, have been subtracted as described in Materials and Methods. To emphasize some of the fine structural details, contours have been superimposed onto each particle image. $n$ denotes the number of particles included in each average. Bright areas represent mass (i.e., protein). Bar, 100 nm (*a–d*).

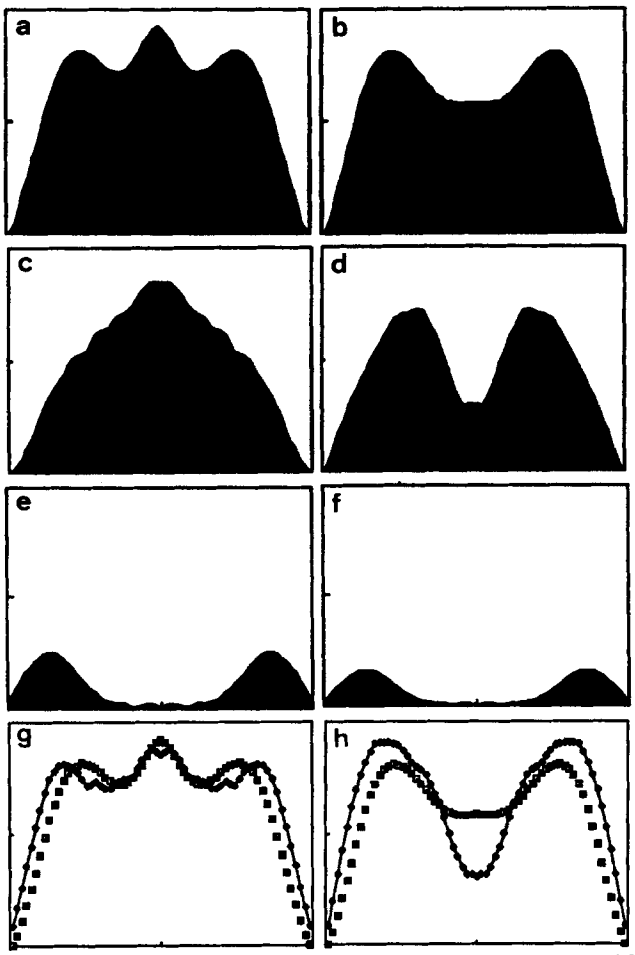


*Figure 7.* Radial mass profiles (RMPs) of averaged intact (*a* and *b*) and detergent-treated (*c–f*) NPCs, obtained by angularly integrating corresponding mass maps (see Fig. 6) over an interval of $\pi$, are all displayed at the same scale. (*a*) Intact NPC with plug, (*b*) intact NPC without plug, (*c*) plug–spoke complex, (*d*) spoke complex, (*e*) heavy ring, and (*f*) light ring. The average contributions of the nuclear envelope (*a* and *b*) and the carbon support film (*c–f*), respectively, have been subtracted as described in Materials and Methods. In *g* and *h* the measured RMPs (delineated by squares) of intact NPCs with (*g*) and without (*h*) plug are compared with the corresponding simulated RMPs (delineated by solid lines with circles); i.e., the intact NPC with plug (*a*) is simulated by the sum of one plug–spoke complex (*c*), one heavy (*e*) and one light (*f*) ring, and the intact NPC without plug (*b*) by the sum of one spoke complex (*d*), one heavy (*e*), and one light (*f*) ring.

contained their cytoplasmic and nucleoplasmic rings, our tilted views of these complexes clearly demonstrate that they have actually lost both rings (Fig. 2), hence the name plug–spoke or spoke complexes.

Detergent treatment of the nuclear envelope is likely to cause alterations beyond dissociation of the intact NPC into several distinct NPC components. It solubilizes the lipids of the nuclear envelope, thereby revealing the underlying nuclear lamina meshwork (Gerace, 1986; Aebi et al., 1986). In addition, removal of the lipid bilayer together with some membrane-bound material appears to significantly increase the surface area of the different NPC components accessible to the negative stain, thus unmasking structural details otherwise buried in the nuclear envelope moiety embracing the intact NPC (see Fig. 8). For example, several fine structural features are identified within the plug–spoke and spoke complex (Fig. 3, *b* and *c*) that are not depicted within the intact NPC (Fig. 3 *a*).

Comparing the characteristic dimensions of unstained/freeze-dried intact and detergent-treated NPCs with those of the corresponding structures after negative staining, we have found them to match within a few percent (see Table I). Furthermore, unstained intact and detergent-treated NPCs after freeze-drying (Figs. 4 and 6) exhibit the same distinct structural features already known from the corresponding negatively stained structures (Figs. 1–3). That these features are generally less pronounced in STEM micrographs is primarily due to the lower inherent contrast of unstained/freeze-dried biological matter, as well as the presence of significant quantum noise coming from the small recording doses (i.e., 50–300 $e^-/nm^2$) employed. This is particularly true for the spokes that are hardly discernible in the STEM images of plug–spoke and spoke complexes (Fig. 4 *f*).

Digitally recorded elastic annular dark-field images directly represent the two-dimensional distribution of projected mass with a theoretical resolution of two pixels. The pixel size was set to either 1.84 or 3.68 nm with the electron beam focused accordingly. Beam current and probe dwelling time were adjusted to obtain total electron doses $\leqslant$300 $e^-/nm^2$, thus keeping beam-induced mass loss <3% (Engel, 1978; Engel et al., 1982). The remaining minor mass loss of the NPC structures was automatically compensated for by assuming identical mass loss kinetics as observed for tobacco mosaic virus coprepared with each sample (Wall, 1979). Nonlinearities due to plural scattering were corrected for sample thicknesses >30 nm: with our experimental set-

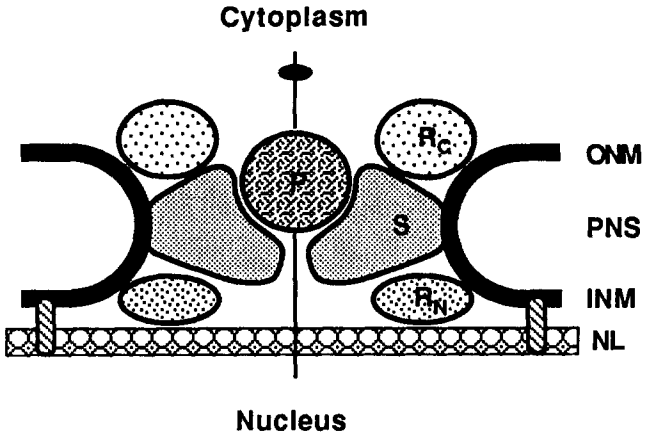


*Figure 8.* Cross-section of our tentative NPC model (*a*) based on experimental CTEM and STEM results yielded in this investigation (cf. Figs. 2, 5, 7 and Table I), and (*b*) incorporating a number of previously published NPC data and models. The central axis marks an eightfold rotational symmetry axis perpendicular to the nuclear membrane plane. The overall shape and dimensions of the distinct NPC components have been drawn such as to approximately reveal the corresponding RMPs displayed in Fig. 7 when projecting their mass thicknesses in a direction parallel to the central axis. For the slight deviations occurring in the central region of the NPC see Discussion. Abbreviations used: *P*, central plug; $R_C$, cytoplasmic ring; $R_N$, nucleoplasmic ring; *S*, spoke; *ONM*, outer nuclear membrane; *INM*, inner nuclear membrane; *PNS*, perinuclear space; *NL*, nuclear lamina.

up the correction for a 50-nm-thick proteinaceous structure supported by a 4-nm-thick carbon film is ~2.5% (Reichelt and Engel, 1984).

The statistical error to be expected from such measurements can be estimated from the actual mass of the structure under investigation (Wall, 1979). Accordingly, an intact NPC is composed of $\sim 9 \cdot 10^6$ atoms of average mass $\langle m \rangle = 13{\cdot}4$ D and an average elastic electron scattering cross-section $\langle \sigma_e \rangle = 10^{-4}$ nm$^2$. When irradiated with a dose of 100 e$^-$/nm$^2$ this structure scatters $9 \cdot 10^4$ electrons from which 69% are collected and counted by the annular detector of our STEM (Engel, 1978). Hence a single NPC generates $6.2 \cdot 10^4$ counts, leading to a quantum noise of ~250 counts. This estimate, however, disregards statistical errors stemming from carbon scattering, and errors due to residual salts, detergent, or small polypeptides adhering to the biological material or sticking to the carbon support film.

As can be gathered from Table I, our experimental data reveal SDs from the mean of ~10%, indicating that the quantum noise as estimated above cannot be the primary source of the observed fluctuations. Thus, our mass measurements reveal an inhomogeneity of the intact NPCs as well as the distinct NPC components together with a significant variability of the background (see mass histograms in Fig. 5), and therefore raise the question about the existence of systematic errors. To this end, we can exclude preferential adsorption of salts, detergent, or small polypeptides to the protein structures, since the mass-per-length measured for tobacco mosaic virus coincided with the theoretical value within 10% (see Engel et al., 1981). In addition, our estimate for the contribution of the embracing nuclear envelope to the mass of intact membrane-bound NPCs (see Materials and Methods) appears to be correct, since their corrected mass (i.e., 124 ± 11 MD) closely matches that of intact but membrane-detached NPCs (i.e., 125 ± 12 MD). Finally, note that the error limits in Table I represent SDs, hence the corresponding errors of the mean are typically 7–15 times smaller because 45–224 measurements have contributed to the respective mean values. As a consequence, the mass differences between plug-containing complexes and those without plug, as well as the mass difference between heavy and light rings are statistically significant.

According to their total masses, two types of rings could be distinguished both exhibiting the same inner and outer diameters and eightfold rotational symmetry (Figs. 4 *b*, 6, *c* and *d*, 7, *e* and *f*; Table I). Because the heavy rings were found almost four times as frequently as the light rings (see Results), it is conceivable that due to the particular preparation procedure used (see Materials and Methods), the heavy rings represent the cytoplasmic and the light rings represent the nucleoplasmic ring of the intact NPC. This interpretation is further supported by the observed asymmetry of edge-on views of intact NPCs sometimes seen in thin-sectioned material where the cytoplasmic ring usually appears more massive than the nucleoplasmic ring (see Fig. 6, Franke [1974]; Fig. 3, Dwyer and Blobel [1976]; Fig. 1, Franke et al. [1981]; Figs. 3, 5, and 8, Scheer et al. [1988]; our own unpublished data).

It was proposed by Unwin and Milligan (1982) that the eight 22-nm particles decorating the cytoplasmic ring of the intact NPC might represent ribosomes, perhaps forming a circular type of polyribosome (Mepham and Lane, 1969). Based on our mass measurements of heavy rings with and without particles we cannot a priori reject this hypothesis. On the one hand, the total mass of 32 MD for the heavy ring comes very close to that of a circular polyribosome, i.e., 33.6 MD when assuming an 80S eukaryotic ribosome mass of 4.2 MD (Alberts et al., 1989) and neglecting any mass for ribosome-connecting material. However, this interpretation seems rather unlikely because the ring dimensions (i.e., width ~30 nm, mean ring diameter ~90 nm) are inconsistent with those of a circular polyribosome (i.e., width ~25 nm, mean ring diameter ~65 nm; see Unwin [1977] for ribosome dimensions). On the other hand, the particles sporadically decorating the heavy rings (Fig. 4 *c*) appear too heavy, i.e., 6.7 MD (see Results), to represent eukaryotic ribosomes, and the same holds true for the 6-MD particles (i.e., the light particles; Table I) often found next to NPC components such as rings (see Fig. 4 *c*). One attempt to clarify this question would involve the quantitative analysis of phosphorus using quantitative electron spectroscopic imaging (ESI; Leapman and Ornberg, 1988) in the heavy and light rings, as well as in the various NPC-related particles.

To evaluate the mass of the central plug, we calculated the mass difference of NPC structures with and without plug to obtain an average difference of 13 MD (see Table I). In all detergent-treated preparations we reproducibly observed particles exhibiting a roughly spherical shape and a mass density typical for proteins. Such particles occurred with a frequency comparable to that of the heavy rings (Figs. 1 *b*, 4, *b* and *c*). A mass analysis of these particles revealed two distinct particle populations, i.e., "heavy" particles (13 MD; Table I) and "light" particles (6 MD; Table I). The heavy particles might possibly represent "detached" central plugs. That the central plug may be a relatively labile structure, i.e., one that easily dissociates from the NPC, is further supported by the presence of significant numbers of intact and detergent-treated NPC structures apparently having lost their central plug both in negatively stained (Fig. 1), as well as in unstained/freeze-dried (Fig. 4) preparations. The question then arises whether the central plug represents an integral component of the NPC, i.e., the "transporter" recently described by Akey and Goldfarb (1989), or whether it represents a distinct particle in transit, i.e., one being transported through the NPC. Its overall size and mass, however, argue against the latter possibility. Furthermore, it is important to note that the central plug does not represent the only structural component within the central area of both intact and detergent-treated NPCs, as the radial mass profiles (RMPs) of intact NPCs as well as plug-spoke and spoke complexes clearly demonstrate (Fig. 7). To this end, the eightfold rotationally symmetrized average of 40 negatively stained spoke complexes (Fig. 3 *c*) unveils some fine-spun material arranged in a ring, possibly representing "inner pore filaments" (Franke, 1974), connecting the eight spokes. It is conceivable that this central structure represents a more tightly bound constituent of the transporter. Finally, it is not clear whether the minor masses depicted inside the heavy and light rings (<5% of the total ring mass; see Fig. 7, *e* and *f*) represent some inherent structural features of the NPC, or are due to a specimen preparation artifact.

The total mass, or the RMPs of the intact NPC both with and without plug (Figs. 7, *g* and *h*) is in good agreement with the respective sums calculated from the measured masses

(Table I), or the RMPs (Fig. 7, *c–f*), of its components (see Fig. 8):

intact NPC with plug (124 MD) = plug-spoke + heavy ring + light ring
= 66 + 32 + 21 MD = 119 MD

intact NPC without plug (112 MD) = spoke + heavy ring + light ring
= 52 + 32 + 21 MD = 105 MD

The slightly lower masses of the sums calculated from the NPC components may indicate some mass loss (<7%) of the components upon detergent treatment. Conversely, the effective mass of the intact NPC may be a few percent lower than the measured 124 MD, i.e., due to some attached material that does not represent an integral part of the NPC. Also, the RMPs of intact NPCs with and without plug compare reasonably well with the corresponding sums computed from the corresponding NPC component RMPs (Fig. 7, *g* and *h*). Despite this few percent uncertainty, these results document that the major components of the intact NPC consist of one heavy and one light ring, and one plug-spoke complex. Last but not least, these STEM measurements bring to an end ongoing speculations about the effective mass of the NPC which have stated values ranging from ≤10 to 160 MD (see Franke, 1974; Fry, 1976; Maul, 1977; Krohne et al., 1978; Blobel, 1985; Gerace and Burke, 1988), and they suggest that the NPC could easily be made of the order of a 100 different polypeptides.

In Fig. 8, a NPC model is proposed, which (*a*) is based on our experimental results including total masses, mass maps, radial mass profiles, and dimensions of unstained/freeze-dried, and dimensions and structural features of negatively stained intact NPCs and distinct NPC components; and (*b*) integrates a number of previously published NPC data and models (see Franke, 1974; Dwyer and Blobel, 1976; Franke et al., 1981; Unwin and Milligan, 1982; Scheer et al., 1988; Akey, 1989; Akey and Goldfarb, 1989). The overall dimensions of this model are 120 nm (i.e., the outer diameter of the NPC proper neglecting the radial arms (Akey, 1989) by ~70 nm (i.e., its overall thickness perpendicular to the nuclear envelope). The eightfold rotationally symmetric spoke complex is sandwiched between a heavy cytoplasmic and a light nucleoplasmic ring and embraces a roughly spherical central plug or transporter. The cross-sectional profile of the spokes has been drawn to be consistent with (*a*) their RMP, (*b*) the physical opening of the NPC (i.e., ~9 nm on the nucleoplasmic side) acting as a molecular sieve, and (*c*) the seemingly weak interaction between the central plug and the surrounding spoke complex. As a consequence, not only the cytoplasmic and nucleoplasmic rings, but also the spokes are asymmetric relative to the nuclear envelope plane. Thus, the resulting structural differences between the cytoplasmic and nucleoplasmic halves of the NPC are consistent with its well-documented functional polarity facilitating vectorial transport of molecules and particles between the nucleus and the cytoplasm.

We would like to thank Ms. H. Frefel, Ms. M. Steiner, and Ms. M. Zoller for their expert photographic work. This work was supported by the M. E. Müller Foundation of Switzerland, grants No. 3.085-0.87 (to U. Aebi) and No. 3.524-0.86 (to A. Engel) awarded by the Swiss National Science Foundation, and the Department of Education of the Kanton Basel-Stadt.

Received for publication 6 September 1989 and in revised form 15 December 1989.

### *References*

Abelson, H. T., and G. H. Smith. 1970. Nuclear pores: the pore-annulus relationship in thin section. *J. Ultrastruct. Res.* 30:558–588.

Aebi, U., J. Cohn, E. L. Buhle, and L. Gerace. 1986. The nuclear lamina is a meshwork of intermediate-type filaments. *Nature (Lond.).* 323:560–564.

Akey, C. W. 1989. Interactions and structure of the nuclear pore complex revealed by cryo-electron microscopy. *J. Cell Biol.* 109:955–970.

Akey, C. W., and D. S. Goldfarb. 1989. Protein import through the nuclear pore complex is a multistep process. *J. Cell Biol.* 109:971–982.

Alberts, B., D. Bray, J. Lewis, M. Raff, K. Roberts, and J. D. Watson. 1989. Molecular biology of the cell. Garland Publishing, Inc., New York/London. 210–211.

Bevington, P. R. 1969. Data reduction and error analysis for the physical sciences. McGraw-Hill Book Company, New York. 235–242.

Blobel, G. 1985. Gene gating: a hypothesis. *Proc. Natl. Acad. Sci. USA.* 82:8527–8529.

Bonner, W. M. 1975*a*. Protein migration into nuclei. I. Frog oocyte nuclei in vivo accumulate microinjected histones, allow entry to small proteins, and exclude large proteins. *J. Cell Biol.* 64:421–430.

Bonner, W. M. 1975*b*. Protein migration into nuclei. II. Frog oocyte nuclei accumulate a class of microinjected oocyte nuclear proteins and exclude a class of microinjected oocyte cytoplasmic proteins. *J. Cell Biol.* 64:431–437.

Buhle, E. L., Jr., B. E. Knox, E. Serpersu, and U. Aebi. 1983. The structure of the $Ca^{2+}$ ATPase as revealed by electron microscopy and image processing of ordered arrays. *J. Ultrastruct. Res.* 85:186–203.

Buhle, E. L., Jr., U. Aebi, and P. R. Smith. 1985. Correlation of surface topography of metal-shadowed specimens with their negatively stained reconstructions. *Ultramicroscopy.* 16:436–450.

DeRobertis, E. M., R. F. Longthorne, and J. B. Gurdon. 1978. Intracellular migration of nuclear proteins in *Xenopus* oocytes. *Nature (Lond.).* 272: 254–256.

Dingwall, C., and R. A. Laskey. 1986. Protein import into the cell nucleus. *Annu. Rev. Cell Biol.* 2:367–390.

Dingwall, C., S. V. Sharnick, and R. A. Laskey. 1982. A polypeptide domain that specifies migration of nucleoplasmin into the nucleus. *Cell.* 30:449–458.

Dworetzky, S. I., and C. M. Feldherr. 1988. Translocation of RNA-coated gold particles through the nuclear pores of oocytes. *J. Cell Biol.* 106:575–584.

Dwyer, N., and G. Blobel. 1976. A modified procedure for the isolation of a pore complex-lamina fraction from rat liver nuclei. *J. Cell Biol.* 70:581–591.

Engel, A. 1978. Molecular weight determination by scanning transmission electron microscopy. *Ultramicroscopy.* 3:273–281.

Engel, A., and J. Meyer. 1980. Preparation of unstained protein structures for mass determination by electron scattering. *J. Ultrastruct. Res.* 72:212–222.

Engel, A., and R. Reichelt. 1988. Processing of quantitative scanning transmission electron micrographs. *Scanning Microscopy Suppl.* 2:285–293.

Engel, A., F. Christen, and B. Michel. 1981. Digital acquisition and processing of electron micrographs using a scanning transmission electron microscope. *Ultramicroscopy.* 7:45–54.

Engel, A., W. Baumeister, and O. W. Saxton. 1982. Mass mapping of a protein complex with the scanning transmission electron microscope. *Proc. Natl. Acad. Sci. USA.* 79:4050–4054.

Feldherr, C. M. 1975. The uptake of endogenous proteins by oocyte nuclei. *Exp. Cell Res.* 93:411–419.

Feldherr, C. M., and S. I. Dworetzky. 1988. The pore complex in nucleocytoplasmic exchange. *In* Nucleocytoplasmic Transport. R. Peters, editor. Academic Press, New York. 127–144.

Feldherr, C. M., E. Kallenbach, and N. Schultz. 1984. Movement of a karyophilic protein through the nuclear pores of oocytes. *J. Cell Biol.* 99:2216–2222.

Franke, W. W. 1974. Structure, biochemistry and functions of the nuclear envelope. *Int. Rev. Cytol. Suppl.* 4:71–236.

Franke, W. W., and U. Scheer. 1970. The ultrastructure of the nuclear envelope of amphibian oocytes: a reinvestigation. *J. Ultrastruct. Res.* 30:288–316.

Franke, W. W., U. Scheer, G. Krone, and E.-D. Jarasch. 1981. The nuclear envelope and the architecture of the nuclear periphery. *J. Cell Biol.* 91: 39s–50s.

Fry, D. J. 1976. The nuclear envelope in mammalian cells. *In* Mammalian Cell Membranes. Vol. 2. G. A. Jameson, and D. M. Robinson, editors. Butterworth Publishers, Stoneham, MA. 197–265.

Gall, J. G. 1967. Octagonal nuclear pores. *J. Cell Biol.* 32:391–399.

Gerace, L. 1986. Nuclear lamina and organization of nuclear architecture. *Trends Biol. Sci.* 11:443–446.

Gerace, L., and B. Burke. 1988. Functional organization of the nuclear envelope. *Annu. Rev. Cell Biol.* 4:335–374.

Harris, J. R. 1974. Some electron microscopic studies on intact nuclear "ghosts" and nuclear membrane fractions. *Phil. Trans. R. Soc. Lond. B. Biol.*

268:109–117.
Harris, J. R. 1978. The biochemistry and ultrastructure of the nuclear envelope. *Biochim. Biophys. Acta.* 515:55–104.
Hoeijmakers, J. H. J., J. H. N. Schel, and F. Wanka. 1974. Structure of the nuclear pore complex in mammalian cells. Two annular components. *Exp. Cell Res.* 87:195–206.
Kartenbeck, J., H. Zentgraf, U. Scheer, and W. W. Franke. 1971. The nuclear envelope in freeze etching. *Adv. Anat. Embryol. Cell Biol.* 45:1–55.
Krohne, G., W. W. Franke, and U. Scheer. 1978. The major polypeptides of the nuclear pore complex. *Exp. Cell Res.* 116:85–102.
Leapman, R. D., and R. L. Ornberg. 1988. Quantitative electron energy loss spectroscopy in biology. *Ultramicroscopy.* 24:251–268.
Maul, G. G. 1977. The nuclear and cytoplasmic pore complex: structure, dynamics, distribution and evolution. *Int. Rev. Cytol. Suppl.* 6:75–186.
Mepham, R. H., and G. R. Lane. 1969. Nucleopores and polyribosome formation. *Nature (Lond.).* 221:288–289.
Milligan, R. A. 1986. A structural model for the nuclear pore complex. *In* Nucleocytoplasmic Transport. R. Peters, and M. Trendelenburg, editors. Academic Press, London. 113–122.
Newport, J. W., and D. J. Forbes. 1987. The nucleus: structure, function and dynamics. A. *Rev. Biochem.* 56:535–565.
Paine, P. L., L. C. Moore, and S. B. Horowitz. 1975. Nuclear envelope permeability. *Nature (Lond.).* 254:109–114.
Reichelt, R., and A. Engel. 1984. Monte Carlo calculations of elastic and inelastic electron scattering in biological and plastic materials. *Ultramicroscopy.* 13:279–294.
Saxton, O. W., J. T. Pitt, and M. Horner. 1979. The SEMPER image processing system. *Ultramicroscopy.* 4:343–354.
Scheer, U., M. -C. Dabauvalle, H. Merkert, and R. Benevente. 1988. The nuclear envelope and the organization of the pore complex. *In* Nucleocytoplasmic Transports. R. Peters, editor. Academic Press, London. 6–25.
Stewart, M., and S. Whytock. 1988. The structure and interactions of components of nuclear envelopes from *Xenopus* oocyte germinal vesicles observed by heavy metal shadowing. *J. Cell Science* 90:409–423.
Unwin, P. N. T. 1977. Three-dimensional model of membrane-bound ribosomes obtained by electron microscopy. *Nature (Lond.).* 269:118–122.
Unwin, P. N. T., and R. A. Milligan. 1982. A large particle associated with the perimeter of the nuclear pore complex. *J. Cell Biol.* 93:63–75.
Wall, J. S. 1979. Mass measurements with the electron microscope. *Scanning Electron Microscopy.* 2:291–302.
Wrigley, N. G. 1968. The lattice spacing of crystalline catalase as an internal standard of length in electron microscopy. *J. Ultrastruct. Res.* 24:454–464.
Wunderlick, F., and V. Speth. 1972. The macronuclear envelope of *Tetrahymena Pyriformis GL* in different physiological states. IV. Structural and functional aspects of nuclear pore complexes. *J. Microscopie (Paris).* 13: 361–382.
Zimmer, F. J., C. Dreyer, and P. Hausen. 1988. The function of the nuclear envelope in nuclear protein accumulation. *J. Cell Biol.* 106:1435–1444.